Biomaterials Science

ROYAL SOCIETY OF CHEMISTRY

PAPER

View Article Online
View Journal | View Issue

Cite this: *Biomater. Sci.*, 2021, **9**, 3162

Pressure-driven spreadable deferoxamine-laden hydrogels for vascularized skin flaps†

Lijun Wu,‡[a,b] Suyue Gao,‡[b,c] Tianlan Zhao,‡[b] Kai Tian,[b] Tingyu Zheng,[b] Xiaoyi Zhang,[a] Liying Xiao,[a] Zhaozhao Ding,[a] Qiang Lu *[a] and David L. Kaplan [d]

Received 12th January 2021,
Accepted 4th March 2021

DOI: 10.1039/d1bm00053e

rsc.li/biomaterials-science

The development of hydrogels that support vascularization to improve the survival of skin flaps, yet establishing homogeneous angiogenic niches without compromising the ease of use in surgical settings remains a challenge. Here, pressure-driven spreadable hydrogels were developed utilizing beta-sheet rich silk nanofiber materials. These silk nanofiber-based hydrogels exhibited excellent spreading under mild pressure to form a thin coating to cover all the regions of the skin flaps. Deferoxamine (DFO) was loaded onto the silk nanofibers to support vascularization and these DFO-laden hydrogels were implanted under skin flaps in rats to fill the interface between the wound bed and the flap using the applied pressure. The thickness of the spread hydrogels was below 200 μm, minimizing the physical barrier effects from the hydrogels. The distribution of the hydrogels provided homogeneous angiogenic stimulation, accelerating rapid blood vessel network formation and significantly improving the survival of the skin flaps. The hydrogels also modulated the immune reactions, further facilitating the regeneration of the skin flaps. Considering the homogeneous distribution at the wound sites, improved vascularization, reduced barrier effects and low inflammation, these hydrogels appear to be promising candidates for use in tissue repair where a high blood supply is in demand. The pressure-driven spreading properties should simplify the use of the hydrogels in surgical settings to facilitate clinical translation.

1. Introduction

Different scaffolds and hydrogels with physical and chemical cues have been developed to fill tissue defects and to stimulate regeneration.[1–3] However, vascularization remains a key challenge for tissue regeneration.[4–6] Growth factors, small molecule drugs, and ions have been loaded into the matrices, providing niches for improved vascularization and tissue restoration.[7–9] Multiple physical regulators, such as micro-nano hierarchical structures, aligned topographies and mechanical cues, have also been fabricated to facilitate angiogenesis *in vivo*, for more rapid tissue recovery.[10] Although these vascularization strategies are effective for bone and dermis where blood vessels induce the ingrowth of new tissues without necrosis, other tissues with a high oxygen demand usually require faster vascularization to prevent necrosis under hypoxic conditions.[11–13]

Skin flaps are widely used to cover skin defects in reconstructive surgeries.[14–16] Unlike the regeneration of dermis, faster angiogenesis is required for skin flaps to reconnect with the wound bed in order to avoid necrosis.[11,17] Growth factor-laden hydrogels and scaffolds have been used to stimulate angiogenesis of tissue flaps through multiple injections, which increases time and cost in terms of clinical applications.[18–20] Recently, self-healing and injectable hydrogels were developed to promote neovascularization of skin flaps, yet multiple injections of the hydrogels are still necessary for skin regeneration.[21–23] These hydrogels were also physical barriers for the wound beds and flaps, partly restricting angiogenesis of the flaps. Homogeneous angiogenic stimulation remains a challenge for these hydrogels. Spreadable hydrogels seem to be a preferable option to overcome this issue; however, only few spreadable hydrogels without the unwanted flowability were developed in regenerative medicine. To overcome these problems, hydrogels with reduced barrier issues and improved vascularization capacity and clinical applicability are preferable. Cell survival is less of an issue

[a]*National Engineering Laboratory for Modern Silk & Collaborative Innovation Center of Suzhou Nano Science and Technology, Soochow University, Suzhou 215123, People's Republic of China. E-mail: lvqiang78@suda.edu.cn; Tel: (+86)-0512-67061649*
[b]*Department of Plastic and Cosmetic Surgery, The Second Affiliated Hospital of Soochow University, Suzhou 215004, P. R. China*
[c]*Department of Dermatology and Cosmetic Surgery, The Affiliated Suzhou Hospital of Nanjing Medical University, Suzhou 215002, Jiangsu, China*
[d]*Department of Biomedical Engineering, Tufts University, Medford, Massachusetts 02155, USA*

†Electronic supplementary information (ESI) available. See DOI: 10.1039/d1bm00053e

‡These authors contributed equally to this work.

when blood vessels and cells are generally below 200 μm apart.[24–26] Therefore, hydrogels that spread to form thin coatings are a good choice to help alleviate physical hindrance. Considering ease of use, pressure-driven spreading of hydrogels can facilitate clinical applications without a negative inefficient impact on workload in the clinic. However, to the best of our knowledge, hydrogels with these anticipated performances have never been reported in previous studies.

Silk fibroin (hereafter referred to as silk) has been used in skin engineering as a promising matrix due to its biocompatibility, biodegradability, low inflammation and tunable mechanical properties.[27–29] Silk scaffolds and hydrogels with nanofibrous–microporous hierarchical structures were developed to improve utility in skin regeneration, with stiffness tuned to 4–7 kPa and with a capacity for vascularization.[30,31] Both vascular endothelial growth factor (VEGF) and small molecule deferoxamine (DFO) were loaded in the matrices and released slowly to stimulate angiogenesis *in vivo*.[32–35] Recently, beta-sheet-rich silk nanofibers (BSNFs) were assembled to form shear-thinning hydrogels that offer improved loading capacity for bioactive molecules. Both hydrophobic and hydrophilic cargoes could be loaded on the nanofibers and exhibited better sustained release behaviors compared to previous silk-based systems.[36–39] Unlike collagen and chitosan hydrogels, these BSNF materials also exhibited a solution–hydrogel transition following increased silk concentration.[1,29,40] The properties suggested a possible balance, where BSNFs exhibit an outstanding spreading capacity but remain in the hydrogel state. Considering their above advantages as wound matrices, BSNF hydrogels are a suitable choice for skin flaps. Unfortunately, injectable BSNF hydrogels with different silk concentrations failed to achieve spreadability without compromising flowability. Further treatment is required to tune the BSNF hydrogels, which will endow them with pressure-driven spreading behaviors. Thus, the goal here was to design spreadable BSNF hydrogels with vascularization capacity, to accommodate the needs identified earlier, with a stimulus of angiogenesis without the unwanted physical barriers for skin flaps.

To simplify clinical applications, pressure-driven spreading is a preferable option for hydrogels involved in skin flap surgery. Spreadable hydrogels with a thickness of about 200 μm should also minimize physical barriers between the wound bed and the skin flap. Here, BSNFs with different silk concentrations were tuned in terms of their rheological properties for spreadable behavior with applied pressure, forming thin coatings with tunable thickness. Previous studies suggested that the enhancement of vascularization and antioxidation is effective in promoting wound healing and accelerating the repair of chronic wounds.[41–43] Deferoxamine (DFO) exhibited angiogenic and antioxidative capacities and could be released slowly from the BSNF-based hydrogels. Therefore, the DFO-laden hydrogels were optimized to improve the vascularization capacity.[32] The DFO-laden hydrogels were then pressed to cover wound defects, and compared to other hydrogel systems.[7,18] Besides the cytocompatibility and vascularization capacity, the hydrogels also exhibited significantly more rapid angiogenesis and reduced necrosis *versus* controls without these features when implanted into skin flap models in rats (Scheme 1).[7,32,44,45]

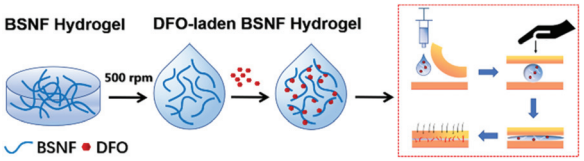

Scheme 1 Overview of the preparation and utility of DFO-laden BSNF hydrogels: after injection, the hydrogel spreads homogeneously under pressure, forming a thin coating with angiogenic capacity.

2. Materials and methods

2.1 Preparation of BSNF hydrogels

The BSNF hydrogels were assembled by a concentration-dilution-thermal incubation process.[32] Raw silk fibers (70 g) were boiled in sodium carbonate solution (0.2%) at 100 °C for 30 min to remove sericin proteins. After drying overnight, the degummed fibers were dissolved in LiBr solution (9.3 M) at 60 °C, dialyzed against water for 72 h, and centrifuged at 9000 rpm for 20 min, obtaining aqueous SF solution with a concentration of about 6 wt%. The silk solution was concentrated for 3–5 d at 40 °C to above 20 wt% and then diluted to 0.3–2 wt%. The diluted solutions were incubated at 60 °C until hydrogels were formed to transform them into beta-sheet-rich silk nanofibers.[30,46] The BSNF hydrogels with different concentrations were then stirred at 500 rpm for 4 h to tune their rheological behaviors.

2.2 Spreading properties of BSNF hydrogels with various concentrations

The pressure exerted by three surgeons on the skin during surgery was measured through a simulated surgery process. A silicone film having similar softness to skin was placed on the tray of the electronic balance. Then the surgeons pressed the silicone film vertically with similar pressure to that applied in real operation. The pressure was measured and maintained in the range of 490 g to 530 g. Therefore, we chose 500 g to simulate the pressure of the surgeon's finger to assess the spreading properties of BSNF hydrogels. To visualize the spreading of BSNF hydrogels, the samples were stained with methylene blue. After the BSNF hydrogels (0.5 ml) were placed under the flaps or between two glass slides, the hydrogels were pressed at 500 g to measure the thickness and spreading area. The spread hydrogels were also imaged after the removal of the pressure to evaluate the spreading stability. In order to test the volume change of the BSNF hydrogel after contact with the tissue fluid, the swelling test was also carried out in PBS solutions at 37 °C. Samples were soaked in PBS (pH7.4) at 37 °C for 0.5, 1, 2, 4, 8, 12 and 24 h. At indicated time points, the samples were collected from the PBS solution, the remaining

solution on the surface of the samples was wiped with a clean tissue paper, and then weighed. The swelling ratio (%) was obtained using the following equation:

$$\text{Swelling ratio } (\%) = (W_t - W_0)/W_0,$$

where W_0 is the initial weight of the hydrogel and W_t is the weight of the hydrogels in PBS at a certain time point.

The rheological behavior of BSNF hydrogels was measured using a rheometer (AR2000, TA Instruments, New Castle, DE).

2.3 Preparation and characterization of DFO-laden BSNF hydrogels

Different amounts of DFO powders (Sigma-Aldrich, Shanghai, China) were added to BSNF hydrogels (1 wt%) directly and stirred at 500 rpm for 4 h. The DFO content in the hydrogels was tuned in the range of 30 μM–180 μM to optimize the vascularization outcomes. All DFO-laden hydrogels were sterilized (60Coγ, 25 kGy) before cell culture *in vitro* and wound healing *in vivo*. Raman spectra were used to confirm the loading of DFO in the hydrogels, measured using a confocal Raman spectrometer (LabRam HR800, HORIBA, France) with a 633 nm excitation wavelength. The samples were assessed on a 20 mm cone plate (Ti, 20/1°) over a frequency range from 1 to 1000 rad s^{-1} at 37 °C. The viscosity of the BSNF hydrogels and DFO-laden BSNF hydrogels against shear rates was analyzed for dynamic viscosity.[32,39] The BSNF hydrogels were pushed through a needle (22 G) at 1.5 N to assess injectability.

2.4 Release behavior of DFO from hydrogels

To investigate the release behavior of DFO from hydrogels, 2 ml of DFO-laden BSNF hydrogels were transferred into a dialysis tube (Thermal Scientific, MWCO 3500) and soaked in 10 ml of phosphate buffered saline (PBS) solution for 40 days. At designed time points, 1 mL was collected and immediately replaced with an equal amount of fresh PBS. The collected supernatants were combined with ferric chloride (6 mM) at a volume ratio of 1 : 1. The DFO release was obtained by detecting absorbance at 485 nm using a multiscan spectrometer (BioTek, USA) as previously reported.[47]

2.5 Cell culture

Endothelial cells were cultured *in vitro* to assess the cytocompatibility of the hydrogels. Human umbilical vein endothelial cells (HUVECs) were obtained from the Cell Bank of the Chinese Academy of Sciences (Shanghai, China). The CCK-8 assay was used to evaluate the proliferation of HUVECs on the hydrogels. The cells were seeded on the surface of DFO-laden BSNF hydrogels with different amounts of DFO (DFO concentrations, 30 μM–180 μM) at 5×10^3 cells per well using 96-well plates. As a control, the cells were also cultured in the medium with an equal amount of free DFO and on the surface of DFO-free BSNF hydrogels. After culturing for 1, 2 and 3 days, the cells were incubated with CCK-8 solution in a cell incubator for 2 h and the absorbance at 450 nm was measured using the multiscan spectrometer.[48,49]

2.6 Tube formation on the DFO-laden BSNF hydrogels

The vascularization capacity of DFO-laden BSNFs was evaluated *in vitro* using a tube formation assay. Matrigel (500 μL per well, BD Biosciences, USA) was coated on the BSNF hydrogels in a 24-well plate according to a reported work.[47] HUVECs were co-cultured on the surface with a cell density of 3×10^4 cells per each well. After culturing for 12 h, tube formation of HUVECs was observed using an inverted microscope (Axio Vert.A1, Carl Zeiss, Germany) and analyzed using ImageJ.

2.7 *In vivo* flap model

All animal procedures were performed in accordance with the Guidelines for Care and Use of Laboratory Animals of Soochow University and approved by the Animal Ethics Committee of Soochow University. Rats used were maintained under specific pathogen-free conditions (SPF). Twenty-four Sprague-Dawley (SD) adult male rats (weight 200 ± 50 g) were randomly divided into three groups (n = 8): control group, DFO-free BSNF hydrogel group and DFO-laden BSNF hydrogel group (DFO, 60 μM). The rats were anesthetized with 4% chloral hydrate (intraperitoneal injection, 1 mL per 100 g), followed by shaving to remove the hair from their back using an electric clipper. The random flap model was also used in our spreadable hydrogels, but excellent flap survival (near 100%) was observed for both DFO-free and DFO-laden hydrogels (data not shown). A different flap model with less blood supply is required for our present study. The iliolumbar vessels are often attached in the random flap, which then influences the necrotic ratio. Recently, a ping pong-shaped flap with a narrower width and longer length was designed to avoid vascular penetration. Repeatable distal necrosis was achieved for the ping pong-shaped flap, suggesting its advantages in evaluating the survival of skin flaps.[50,51] Therefore, a ping pong-shaped flap model was used in the present study to reveal the function of the hydrogels in stimulating the blood vessel formation and reducing the necrosis. Intraoperative observation of the ping pong-shaped flap revealed the blood vessel free state of the pedicle.[51] A caudally based dorsal flap with a racket shape (pedicle: 1.0 × 3.0 cm, flap: d = 3.0 cm) was incised with a scalpel. The full-thickness skin was raised to separate from the deeper muscular fascia, leaving an unincised pedicle (width, 1 cm). No axial vessel passed through the pedicle. The hydrogels were pushed under the flap with a syringe, following by suturing the flap closed. The sutured flaps were pressed by hand to spread the hydrogel, ensuring homogeneous distribution of the hydrogels under the flaps (Fig. S1†). Finally, the flaps were covered with sterile gauze. The rats were housed individually without antibiotics.

2.8 Evaluation of flap survival and blood perfusion

At 1, 3 and 7 days post-operation, photographs of the flaps were taken and analyzed using a digital camera (Canon 5D Mark IV, Japan). The necrotic areas were evaluated through the color, temperature, capillary reaction and elasticity of the flap using the standard methods, and were evaluated individually

by two dermatological pathologists using a double-blind method.[11,44,52] The percentage of skin necrosis was calculated by dividing the necrotic area by the round area. Blood perfusion of the flap was measured using the infrared thermal imager (Ti450, Fluke, China) after 3 and 7 days post-operation.

2.9 Evaluation of neovascularization and inflammation

After 7 days post-surgery, the rats were euthanized for flap sample collection. The flaps and adjacent tissues were harvested and fixed with 4% paraformaldehyde. The samples were stained with Hematoxylin and Eosin (H&E) to evaluate survival and angiogenesis. Immunofluorescence staining for CD31 (1 : 100 dilution, Ab28364, Abcam) was performed to evaluate the blood vessel formation and CD68 and CD206 immunofluorescence staining was performed to investigate the inflammatory responses.

2.10 Statistical analysis

The data were statistically analyzed using SPSS v.16.0 software. One-way ANOVA was performed to compare the mean values of the data. $p < 0.05$ was considered statistically significant.

3. Results and discussion

Multiple strategies have been developed to design hydrogels with vascularization capacity for reducing necrosis.[17,21,53–55] The use of hydrogels are often incompatible with flap surgery, thereby, limiting clinical applications. Although previous hydrogels containing vascularization stimulators promoted angiogenesis and reduced necrosis, these hydrogels were also physical barriers for the wound beds and flaps, partly restricting angiogenesis of the flaps.[42,53] Multiple injections of hydrogels also resulted in heterogeneous outcomes in terms of skin flap regeneration.[20,21,54] Ideally, hydrogels with vascularization cues should distribute homogeneously at the interface of the wound bed and the flap, forming a thin coating with a thickness below 200 μm to minimize barrier influence.

BSNFs composed of beta-sheet-rich conformation had a high negative charge density, providing shear-thinning properties and resulting in solution–hydrogel transitions at different silk concentrations.[27,28,32,46,56] Spreadability of the hydrogel could facilitate its homogeneous distribution in skin flaps, but also results in the flowability that worsens the function. It remains a great challenge to develop spreadable hydrogels without the unwanted flowability. To reveal the balance of spreading and adhesion of the BSNF materials, the BSNFs assembled at different silk concentrations in the range of 0.3–2%. Although injectable DFO-laden silk hydrogels have been developed in our previous studies to accelerate wound healing,[32] BSNF hydrogels with different silk concentrations failed to achieve the spreadability without compromising flowability. The negative charge repulsion could also rearrange the aggregation of the BSNFs after the stirring treatment, which further tuned the flowability and spreading capacity of the hydrogels. Therefore, solid BSNF hydrogels were treated with a stirring process to change their rheological behaviors. After the treatment, the pressure-driven spreadable hydrogels without the unwanted flowability were prepared, which would facilitate their application in skin flaps (Fig. S2†). The pressure of the surgeon's finger during surgery is usually in the range of 490–530 g (Fig. S3†); the BSNF hydrogels were pressed at 500 g to evaluate the spreading and adhesion (Fig. 1a–c). For the BSNFs with concentrations below 1%, flowability resulted in the loss of BSNFs after pressing. When the SF concentration was increased to 1%, the BSNF hydrogels easily spread and formed thin coatings (Fig. 1d). The coatings remained stable without shrinking or contraction after the removal of the pressure, suggesting that the hydrogels would distribute at the interface of the wound bed and flap in a homogeneous fashion. The thickness of the coating was investigated to evaluate the minimization as a physical barrier, and hydrogels with a silk concentration of 1% formed a coating of about 178.6 ± 11.3 μm (below 200 μm) (Table 1). Swelling behaviors of the hydrogels were studied to evaluate the volume changes of BSNF hydrogels *in vitro*. The results showed that BSNF hydrogels remained stable without significant volume changes (<10%) in the PBS solution (Fig. S4†). Similar to the BSNF hydrogels without stirring treatment, the treated hydrogels could be injected with needles (22 G) easily, suggesting their injectability (Fig. S5†). Therefore, the hydrogels with a silk concentration of 1 wt% were used to load DFO to promote angiogenesis of the flaps.

To optimize the cytocompatibility and vascularization capacity of the hydrogels, different amounts of DFO were loaded in the BSNFs directly for *in vitro* cell culture. The Raman spectra of DFO-laden hydrogels had typical peaks of DFO and silk (584 cm^{-1}, 1050 cm^{-1}, 1350 cm^{-1} and 1450 cm^{-1} for DFO and 1064 cm^{-1}, 1232 cm^{-1} and 1665 cm^{-1} for silk),

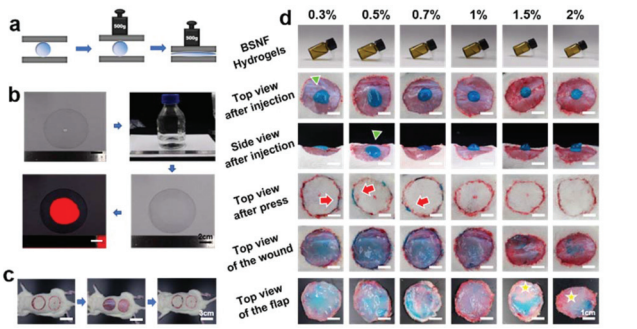

Fig. 1 (a) Schematic diagram of the pressure-driven hydrogels under 500 g pressure *in vitro*. (b) 0.5 ml BSNF hydrogels were spread to form uniform thin coatings at 500 g pressure between glass plates. (c) Schematic diagram of 10 cm^2 full-thickness skin defect on the back of rats. After 0.5 ml BSNF materials with different concentrations were injected on the wound, the skin was reapplied to cover the wound bed and pressed to test the spreading of the hydrogels. (d) Spreading and adhesion properties of the BSNF materials with different concentrations. Silk nanofiber hydrogels were marked with methylene blue. (→ means the hydrogels overflowed from the edges of the skin, Δ means a high degree of fluidity of the hydrogels, ☆ means shrinking of the hydrogels after the removal of pressure).

Table 1 The area and thickness of the coating formed between two glass slides under 500 g pressure. Every sample was measured five times; the difference between every two groups was significant ($p < 0.05$)

Silk (%)	Coating ($cm^2 \pm SD$)	Thickness ($\mu m \pm SD$)
0.3	78.5 ± 2.5	63.7 ± 16.7
0.5	63.6 ± 1.9	78.6 ± 12.9
0.7	36.2 ± 2.3	138.1 ± 15.2
1.0	28.0 ± 1.8	178.6 ± 11.3
1.5	13.8 ± 1.7	361.3 ± 9.2
2.0	9.6 ± 1.2	519.8 ± 5.7

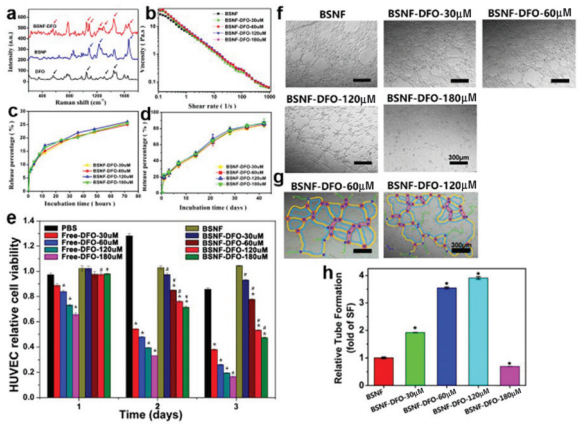

Fig. 2 Characterization of BSNF hydrogels. (a) Raman spectra; (b) viscosity of the hydrogels before and after loading DFO; (c and d) DFO release properties *in vitro* of the 1% BSNF hydrogels in 3 days and 42 days; (e) cell viability of HUVECs for 3 days; (f) tube formation of HUVECs at 12 h, scale bars are 300 μm; and (g and h) tube length of HUVECs. Statistically significant, $*P \leq 0.05$ compared with the control group, $\#P \leq 0.05$ compared with the cells cultured in free DFO solutions of the same concentration.

confirming the successful loading of DFO (Fig. 2a). Similar to pure BSNF hydrogels, the DFO-laden hydrogels retained their shear-thinning behavior and exhibited a slight increase of viscosity. The hydrogels with different amounts of DFO had similar viscoelasticity without significant differences (Fig. 2b). The results suggested that the introduction of DFO did not influence the spreading. Different amounts of DFO were released slowly from the hydrogels over 40 days, suggesting that sustained vascularization stimulation could be achieved with the hydrogels (Fig. 2c and d). A previous study revealed that the sustained release of DFO from the BSNF hydrogels stimulated quick angiogenesis at the dermal wound sites, superior to other DFO-laden biomaterial systems.[32,47] Therefore, these BSNF hydrogels with vascularization potential were developed without compromising the original, beneficial mechanical properties.

DFO-laden hydrogels have been used to stimulate dermal regeneration, considering vascularization and cytocompatibility, and BSNF hydrogels with 120 μm DFO were considered better matrices for the dermal defect repair.[32] Unlike the dermis application in our prior studies, the skin flap model requires hydrogels with improved biocompatibility and vascularization for faster reconnection with the wound bed. Human umbilical vein endothelial cells (HUVECs) were cultured on different DFO-laden hydrogels to assess the cytocompatibility and vascularization capacity *in vitro*. Free DFO exhibited significant toxicity when the concentration of DFO was above 30 μM. When the cells were cultured for 3 days, the viability of HUVECs was below 40%. These results suggested that direct injection of DFO was inappropriate for skin flap regeneration. The loading of DFO in BSNF hydrogels significantly attenuated the toxicity of DFO, achieving higher cell viability on the DFO-laden hydrogels (Fig. 2e). However, significant cell cytotoxicity remained for the DFO-laden hydrogels when the DFO amounts were above 60 μM where the viability of HUVECs was below 60% after being cultured for 3 days. More than 75% of the HUVECs remained viable on the hydrogels at the DFO concentration of 60 μM, suggesting the acceptable cytocompatibility of the DFO-laden hydrogels. DFO as an effective angiogenic drug has been used to facilitate blood vessel formation in various tissue regeneration studies *in vitro* and *in vivo*.[47,57–59] Since the vascularization capacity of DFO-laden hydrogels has been investigated extensively in our recent study,[32] the *in vitro* vascularization of the hydrogels with different amounts of DFO was evaluated using the tube-formation assay. Although the longest tubes from the HUVECs appeared in the hydrogels with the DFO concentration of 120 μM, many tubes also formed in the hydrogels with the DFO concentration of 60 μM (Fig. 3f, g and h), showing a slight decrease of vascularization (within 10%). Considering acceptable cytocompatibility and comparable vascularization capacity, the BSNF hydrogels containing 60 μM DFO were selected as better matrices to stimu-

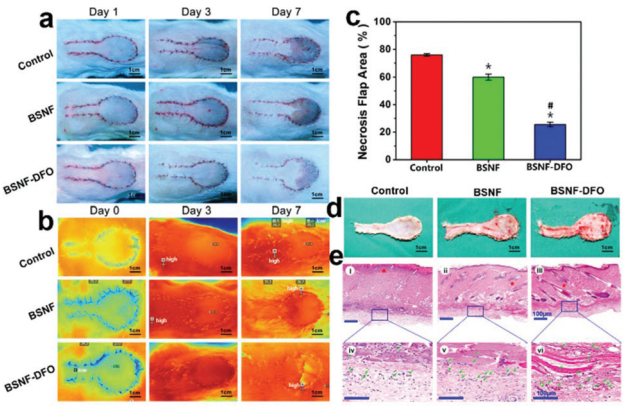

Fig. 3 Skin flap regeneration treated with various samples. (a) Digital photographs of the flaps at days 1, 3, and 7 post operation; (b) blood perfusion of the flaps measured using an infrared thermal imager laser at days 0, 3, and 7 post-operation; and (c) quantitative analysis of flap necrosis using ImageJ software at day 7. Statistically significant, $*P \leq 0.05$ compared with the control group, $\#P \leq 0.05$ compared with the SF group. (d) The detached flaps at day 7 from different groups. (e) Blood vessels in the base and H&E staining of the flaps at day 7, scale bars are 100 μm. (Δ means inflammation of the flap, ☆ means hair follicles, sweat glands and other skin appendages, → means microvessels).

late the vascularization of skin flaps and were subsequently used in the *in vivo* rat models.

The random flap model in rats is usually used to evaluate the influence of the hydrogels with vascularization capacity on flap regeneration.[11,54,60] Necrosis appears at the distal end of the flap because of inferior blood supply. Although the quality of the regenerated flap could be evaluated based on angiogenesis density and necrosis area, more objective evaluation remains a challenge since little necrosis appears in the random flap model without the hydrogel treatment.[41,61] The random flap model was also used in our spreadable hydrogels, but excellent flap survival (near 100%) was observed for both DFO-free and DFO-laden hydrogels (data not shown). A different flap model with less blood supply is required for our present study. The iliolumbar vessels are often attached in the random flap, which then influences the necrotic ratio. Recently, a ping pong-shaped flap with a narrower width and longer length was designed to avoid vascular penetration. Repeatable distal necrosis was achieved for the ping pong-shaped flap, suggesting its advantages in evaluating the survival of skin flaps.[50,51] Therefore, a ping pong-shaped flap model was used in the present study to reveal the function of the hydrogels in stimulating the blood vessel formation and reducing the necrosis. Intraoperative observation of the ping pong-shaped flap revealed the blood vessel free state of the pedicle (Fig S6†). Developing a modified flap model with less blood supply is necessary to reveal the function of the hydrogels in stimulating the blood vessel formation and reducing the necrosis. Therefore, a ping pong-shaped flap model in rats was used in the present study.[50,51] Through tuning the length of the rectangle area, more necrosis was observed and it occurred in most of the round area when the length of the rectangle was 5 cm (Fig. S6†). Since the function of the hydrogels used could be assessed easily through the ratio of necrosis in the round zone, the ping pong-shaped flap is a better model to study the stimulating function of the hydrogels in skin flap regeneration. Therefore, the DFO-laden hydrogels were implanted under the modified ping pong-shaped flap (10 cm^2) and spread by pressing the flap.

The *in vitro* pressure of the hydrogels with glass panels revealed that 0.3 ml of hydrogels (1 wt%) could occupy 10 cm^2 area, forming a thin coating with a thickness of about 178 μm. Various volumes of hydrogels were implanted under the flap to determine a suitable amount of the hydrogel for the flap model *in vivo* and above 0.5 ml was identified (Fig. S7†). The H&E images further revealed that the thickness of the hydrogel at the interface of the wound beds and flaps were 120 μm, 160 μm, 240 μm, and 470 μm after 0, 0.5 ml, 1 ml, and 2 ml of the hydrogels were implanted under the flap, respectively (Fig. S7†). The necrosis area increased with the higher amounts of the hydrogel, reflecting the impact as a physical barrier effect (above 200 μm).[24–26,62] Therefore, 0.5 ml of the hydrogel could cover the flap area with suitable thickness and was used to induce angiogenesis *in vivo*.

DFO-laden hydrogels with different amounts of DFO (0.5 ml) were also implanted under the flap of the rats, and the best viability of the flaps was achieved for the groups with a DFO concentration of 60 μM (Fig. S8†). Therefore, the DFO-laden hydrogels with a DFO concentration of 60 μM were used in the *in vivo* studies. To reveal the stimulating effect of the DFO-laden hydrogels on angiogenesis, the same amount of normal saline and DFO-free BSNF hydrogels (0.5 ml) were used as controls and implanted under the flaps. Compared to the blank control, the laser speckle contrast images showed a significantly lighter color in the flap area for both the DFO-laden and DFO-free BSNF hydrogel groups after the surgery (Fig. 3a and b). The results confirmed that the hydrogels occupied the interface between the wound bed and the flap, in contrast to the punctate distribution in the previous hydrogel systems.[9,21,23] At day 3 after the surgery, almost the whole of the round area of the flap in the blank group showed a lighter color than the surrounding regions, while about 25% of the round part in the DFO-free hydrogel group retained the same color with normal tissues. The results indicated that the BSNF itself stimulated angiogenesis, resulting in improved blood flow under the flap. The vascularization capacity was further improved after the introduction of DFO. The whole of the flap region retained a similar color with the surrounding tissues, indicating the best angiogenesis in the DFO-laden hydrogel group. After 7 days, the color difference became more evident where the best result was achieved in the DFO-laden hydrogel group (Fig. 3a). Necrosis and scabbing were consistent with the laser speckle contrast images. At day 7 after operation, the necrosis area in the blank group was 75% and then decreased to 60% in the DFO-free hydrogel group. The vascularization capacity of the DFO-laden hydrogels reduced necrosis. Only 30% of the round region was observed with necrosis and 70% of the flap successfully survived and had the same appearance with the normal surrounding tissues (Fig. 3c). Although it is difficult to compare with the previous hydrogel systems due to different flap models,[18–20] the DFO-free hydrogel has achieved a comparable flap survival in the random flap model to that of previously reported works, but was inferior to the DFO-laden hydrogel group in the ping pong-shaped flap model, suggesting possible better performances of the DFO-laden hydrogels. The results suggested that the DFO-laden hydrogels stimulated blood vessel formation and improved flap survival.

The skin flaps were peeled off at day 7 after the implantation to reveal blood vessel formation (Fig. 3d). Few blood vessels appeared under the flap in the blank group, indicating inferior angiogenesis. New blood vessels formed under the flap treated with DFO-free BSNF hydrogels, confirming the promoting effect of silk nanofibers on neovascularization. The loaded DFO further stimulated rapid angiogenesis. Rich blood vessel networks distributed homogeneously under the flap in the DFO-laden hydrogel group, which further improved the survival of the flap. H&E staining was performed to evaluate micro-vessel formation at the interface of the wound bed and the flap (Fig. 3e). Few fragile micro-vessels appeared under the blank control flap, which confirmed the inferior blood supply. No SF aggregates were observed below the flap treated with DFO-free hydrogels, suggesting that the nanofibers distributed homogeneously without aggregation. Although the number of vessels increased in the DFO-free hydrogel groups than that of

the control, significantly higher neo-vessels were further regenerated in the DFO-laden hydrogel group (Fig. 4a). Different regions of the round area were investigated and they showed similar angiogenesis. The results revealed that the implanted DFO-laden hydrogels provided homogeneous angiogenic stimulated niches for the skin flaps, an improvement over the previous hydrogel systems.[8,20,21] CD31 immunohistochemical staining images further clarified the density and morphology of the formed vessels. The DFO-laden hydrogel group showed 108 vessels per cm^2, 3 times higher than in the blank group and 1.5 times higher than in the DFO-free hydrogel group. The diameters of the main vessels in the DFO-laden hydrogel group were about 8.6 μm, 1.8 times larger than in the DFO-free hydrogel group, suggesting better and mature blood vessel networks in the DFO-laden hydrogel group (Fig. 4a and c). Therefore, the DFO-laden hydrogels provided the anticipated angiogenic stimulation.

Previous hydrogels with vascularization capacity usually induce inflammation due to foreign body reactions, weakening vascularization in the skin flap.[63–65] Compared to other materials, silk has a lower inflammatory reaction after implantation, strengthening biomedical utility in tissue regeneration.[66–69] DFO regulated inflammatory reactions and angiogenesis to accelerate the healing of diabetic chronic wounds.[9,70–73] Thus, DFO-laden SF hydrogels could minimize foreign body reactions and further improve survival of skin flaps. The macrophage density under the flap was measured by immunohistochemical staining (Fig. 4b). Compared with the blank control group, the number of macrophages was significantly decreased following the use of BSNF hydrogels and then the introduction of DFO. Besides the lower macrophage density, the DFO-laden hydrogels modulated the M1–M2 phenotype of macrophages. A significantly higher ratio of M2 macrophages appeared in the DFO-laden hydrogel group compared to both the blank and DFO-free hydrogel groups (Fig. 4d and e). Therefore, the DFO-laden hydrogels helped to tune the inflammatory behavior, which further accelerated skin flap regeneration. Unlike the previously reported hydrogels with vascularization capacity,[21,54] the present work developed a pressure-driven spreadable hydrogel to provide homogeneous angiogenic stimulation for skin flaps. The hydrogels stimulated angiogenesis and tuned inflammation, significantly improving the survival of the flap. The spreadable property minimized the physical barrier effect of the hydrogels on growing tissues.

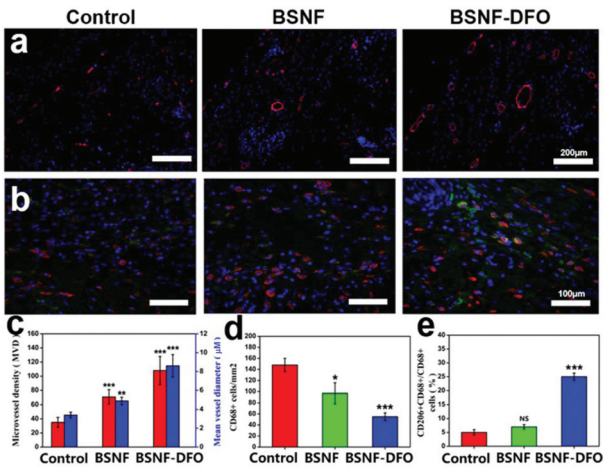

Fig. 4 (a) Immunofluorescence staining of neovascularization of different treatment groups, CD31 (red) and DAPI (nuclei; blue). (b) Immunoregulation at the flap sites when treated with different groups for 7 days. Macrophages are marked with a pan-marker CD68 (green), M2 phenotype was marked with the marker CD206 (red). (c) The microvessel density (MVD) and mean vessel diameter of CD31 + vessels; (d) CD68 + macrophage number per mm^2; and (e) the percentage of M2 phenotype macrophages over total CD68 + macrophages. Data are presented as mean ± SD; $n = 6$, $^*P \leq 0.05$, $^{**}P \leq 0.01$, and $^{***}P \leq 0.001$.

4. Conclusions

The spreading and adhesion properties of BSNF hydrogels were tuned by changing the SF concentration to achieve spreadable hydrogels suitable for skin flap regeneration. DFO was loaded on the BSNF nanofibers to endow the hydrogels with vascularization capacity. The hydrogels occupy the flap region through simple pressing to provide homogeneous angiogenic stimulation, improving the survival of the flap. The thin hydrogel coatings that were formed minimized the physical barrier effects and modulated the inflammatory behavior, further accelerating flap regeneration. The vascularization capacity, inflammation modulation and spreading properties suggest that these DFO-laden hydrogels are promising candidates for flap regeneration and also suitable for other tissues with high blood supply demand.

Conflicts of interest

There are no conflicts to declare.

Acknowledgements

The authors thank the National Key R&D Program of China (2016YFE0204400) and the NIH (P41EB027062). We also thank the Postgraduate Research & Practice Innovation Program of Jiangsu Province (KYCX20_2664), the Project of Natural Science Research in Universities of Jiangsu Province (16KJB320010), the Suzhou Science and Education Program for Promoting Health (KJXW2016015), the 2019 Suzhou City Health Young Talents "National Tutor System" Training Program and the Doctor Scientific Pre-hospital Research Fund (SDFEYBS1805 and SDFEYGJ2013) for supporting this work.

References

1 F. M. Chen and X. Liu, *Prog. Polym. Sci.*, 2016, **53**, 86–168.
2 L. Roseti, V. Parisi, M. Petretta, C. Cavallo, G. Desando, I. Bartolotti and B. Grigolo, *Mater. Sci. Eng., C*, 2017, **78**, 1246–1262.

3 X. Zhao, Q. Lang, L. Yildirimer, Z. Y. Lin, W. Cui, N. Annabi, K. W. Ng, M. R. Dokmeci, A. M. Ghaemmaghami and A. Khademhosseini, *Adv. Healthcare Mater.*, 2016, **5**, 108–118.
4 M. T. Ngo and B. A. C. Harley, *Biomaterials*, 2020, **255**, 120207.
5 G. Eke, N. Mangir, N. Hasirci, S. MacNeil and V. Hasirci, *Biomaterials*, 2017, **129**, 188–198.
6 S. Kargozar, F. Baino, S. Hamzehlou, R. G. Hill and M. Mozafari, *Trends Biotechnol.*, 2018, **36**, 430–444.
7 M. S. Lee, T. Ahmad, J. Lee, H. K. Awada, Y. Wang, K. Kim, H. Shin and H. S. Yang, *Biomaterials*, 2017, **124**, 65–77.
8 K. L. Zhou, Y. H. Zhang, D. S. Lin, X. Y. Tao and H. Z. Xu, *Sci. Rep.*, 2016, **6**, 18945.
9 L. Kong, Z. Wu, H. Zhao, H. Cui, J. Shen, J. Chang, H. Li and Y. He, *ACS Appl. Mater. Interfaces*, 2018, **10**, 30103–30114.
10 M. A. M. Jahromi, P. S. Zangabad, S. M. M. Basri, K. S. Zangabad, A. Ghamarypour, A. R. Aref, M. Karimi and M. R. Hamblin, *Adv. Drug Delivery Rev.*, 2018, **123**, 33–64.
11 X. Sun, Q. Lang, H. Zhang, L. Cheng, Y. Zhang, G. Pan, X. Zhao, H. Yang, Y. Zhang, H. A. Santos and W. Cui, *Adv. Funct. Mater.*, 2017, **27**, 1604–1617.
12 C. B. Thompson, *Cell*, 2016, **167**, 9–11.
13 T. Vasilenko, M. Slezak, M. Novotny, I. Kovac, J. Durkac, I. Tomkova, N. Torma, A. Vrzgula, L. Lenhardt, M. Levkut and P. Gal, *Aesthetic Plast. Surg.*, 2013, **37**, 1003–1009.
14 Y. X. Zhang, T. J. Hayakawa, L. S. Levin, G. G. Hallock and D. Lazzeri, *Plast. Reconstr. Surg.*, 2016, **137**, 1018–1030.
15 G. I. Taylor, R. J. Corlett, S. C. Dhar and M. W. Ashton, *Plast. Reconstr. Surg.*, 2011, **127**, 1447–1459.
16 L. Li, T. L. ten Hagen, M. Hossann, R. Suss, G. C. van Rhoon, A. M. Eggermont, D. Haemmerich and G. A. Koning, *J. Controlled Release*, 2013, **168**, 142–150.
17 M. W. Laschke and M. D. Menger, *Biotechnol. Adv.*, 2016, **34**, 112–121.
18 X. G. Xie, M. Zhang, Y. K. Dai, M. S. Ding and S. D. Meng, *Exp. Ther. Med.*, 2015, **10**, 954–958.
19 D. Chicharro-Alcantara, M. Rubio-Zaragoza, E. Damia-Gimenez, J. M. Carrillo-Poveda, B. Cuervo-Serrato, P. Pelaez-Gorrea and J. J. Sopena-Juncosa, *J. Funct. Biomater.*, 2018, **9**, 10.
20 W. Li, M. Enomoto, M. Ukegawa, T. Hirai, S. Sotome, Y. Wakabayashi, K. Shinomiya and A. Okawa, *Plast. Reconstr. Surg.*, 2012, **129**, 858–866.
21 X. Mao, R. Cheng, H. Zhang, J. Bae, L. Cheng, L. Zhang, L. Deng, W. Cui, Y. Zhang, H. A. Santos and X. Sun, *Adv. Sci.*, 2019, **6**, 1801555.
22 X. Zhao, H. Wu, B. Guo, R. Dong, Y. Qiu and P. X. Ma, *Biomaterials*, 2017, **122**, 34–47.
23 Y. Liang, X. Zhao, T. Hu, B. Chen, Z. Yin, P. X. Ma and B. Guo, *Small*, 2019, **15**, e1900046.
24 P. A. Shiekh, A. Singh and A. Kumar, *ACS Appl. Mater. Interfaces*, 2018, **10**, 18458–18469.
25 M. Lovett, K. Lee, A. Edwards and D. L. Kaplan, *Tissue Eng., Part C*, 2009, **15**, 353–370.
26 J. Rouwkema, N. C. Rivron and C. A. van Blitterswijk, *Trends Biotechnol.*, 2008, **26**, 434–441.
27 C. Vepari and D. L. Kaplan, *Prog. Polym. Sci.*, 2007, **32**, 991–1007.
28 X. Dong, Q. Zhao, L. Xiao, Q. Lu and D. L. Kaplan, *Biomacromolecules*, 2016, **17**, 3000–3006.
29 Y. Cao and B. Wang, *Int. J. Mol. Sci.*, 2009, **10**, 1514–1524.
30 G. Lu, Z. Ding, Y. Wei, X. Lu, Q. Lu and D. L. Kaplan, *ACS Appl. Mater. Interfaces*, 2018, **10**, 44314–44323.
31 Q. Lu, S. Bai, Z. Ding, H. Guo, Z. Shao, H. Zhu and D. L. Kaplan, *Adv. Mater. Interfaces*, 2016, **3**, 1500687.
32 Z. Ding, M. Zhou, Z. Zhou, W. Zhang, X. Jiang, X. Lu, B. Zuo, Q. Lu and D. L. Kaplan, *ACS Biomater. Sci. Eng.*, 2019, **5**, 4077–4088.
33 Q. Wang, Y. Zhang, B. Li and L. Chen, *J. Mater. Chem. B*, 2017, **5**, 6963–6972.
34 Y. Zhang, J. Huang, L. Huang, Q. Liu, H. Shao, X. Hu and L. Song, *ACS Biomater. Sci. Eng.*, 2016, **2**, 2018–2025.
35 B. Wang, X. Lv, S. Chen, Z. Li, J. Yao, X. Peng, C. Feng, Y. Xu and H. Wang, *Cellulose*, 2017, **24**, 5013–5024.
36 Y. Sang, M. Li, J. Liu, Y. Yao, Z. Ding, L. Wang, L. Xiao, Q. Lu, X. Fu and D. L. Kaplan, *ACS Appl. Mater. Interfaces*, 2018, **10**, 9290–9300.
37 L. Xiao, G. Lu, Q. Lu and D. L. Kaplan, *ACS Biomater. Sci. Eng.*, 2016, **2**, 2050–2057.
38 W. Cheng, Z. Ding, X. Zheng, Q. Lu, X. Kong, X. Zhou, G. Lu and D. L. Kaplan, *Biomater. Sci.*, 2020, **8**, 2537–2548.
39 X. Zheng, Z. Ding, W. Cheng, Q. Lu, X. Kong, X. Zhou, G. Lu and D. L. Kaplan, *Adv. Healthcare Mater.*, 2020, **9**, e2000041.
40 P. X. Ma, *Adv. Drug Delivery Rev.*, 2008, **60**, 184–198.
41 S. Zhang, J. Hou, Q. Yuan, P. Xin, H. Cheng, Z. Gu and J. Wu, *Chem. Eng. J.*, 2019, **392**, 123775.
42 G. Liu, Z. Bao and J. Wu, *Chin. Chem. Lett.*, 2020, **31**, 1817–1821.
43 Z. Xu, S. Han, Z. Gu and J. Wu, *Adv. Healthcare Mater.*, 2020, **9**, 1901502.
44 D. Qiu, X. Wang, X. Wang, Y. Jiao, Y. Li and D. Jiang, *Am. J. Emerg. Med.*, 2019, **37**, 828–831.
45 X. Sun, R. Zheng, L. Cheng, X. Zhao, R. Jin, L. Zhang, Y. Zhang, Y. Zhang and W. Cui, *RSC Adv.*, 2016, **6**, 9360–9369.
46 H. Wu, S. Liu, L. Xiao, X. Dong, Q. Lu and D. L. Kaplan, *ACS Appl. Mater. Interfaces*, 2016, **8**, 17118–17126.
47 M. Qiu, C. Wang, D. Chen, C. Shen, H. Zhao and Y. He, *Appl. Sci.*, 2016, **6**, 290.
48 R. Ma, Y. Wang, H. Qi, C. Shi, G. Wei, L. Xiao, Z. Huang, S. Liu, H. Yu, C. Teng, H. Liu, V. Murugadoss, J. Zhang, Y. Wang and Z. Guo, *Composites, Part B*, 2019, **167**, 396–405.
49 Q. Wu, J. Deng, D. Fan, Z. Duan, C. Zhu, R. Fu and S. Wang, *Biochem. Pharmacol.*, 2018, **148**, 64–74.
50 L. Wu, T. Zhao, D. Yu, Q. Chen, W. Han, W. Yu and W. Sun, *PLoS One*, 2015, **10**, e0142417.
51 L. Wu, S. Gao, K. Tian, T. Zhao and K. Li, *J. Cosmet. Dermatol.*, 2021, DOI: 10.1111/jocd.13886.

52 F. Lu, H. Mizuno, C. A. Uysal, X. Cai, R. Ogawa and H. Hyakusoku, *Plast. Reconstr. Surg.*, 2008, **121**, 50–58.
53 M. Hihara, N. Kakudo, N. Morimoto, T. Hara, F. Lai, J. Jo, Y. Tabata and K. Kusumoto, *J. Artif. Organs*, 2020, **23**, 348–357.
54 X. Sun, H. Zhang, J. He, R. Cheng, Y. Cao, K. Che, L. Cheng, L. Zhang, G. Pan, P. Ni, L. Deng, Y. Zhang, H. A. Santos and W. Cui, *Appl. Mater. Today*, 2018, **13**, 54–63.
55 W. Zheng, J. Wang, L. Xie, H. Xie, C. Chen, C. Zhang, D. Lin and L. Cai, *J. Mater. Sci. Mater. Med.*, 2019, **30**, 106.
56 C. Guo, C. Li, X. Mu and D. L. Kaplan, *Appl. Phys. Rev.*, 2020, **7**, 011313.
57 P. Holden and L. S. Nair, *Tissue Eng., Part C*, 2019, **25**, 461–470.
58 Y. Ikeda, S. Tajima, S. Yoshida, N. Yamano, Y. Kihira, K. Ishizawa, K. Aihara, S. Tomita, K. Tsuchiya and T. Tamaki, *Atherosclerosis*, 2011, **215**, 339–347.
59 X. Jiang, A. V. Malkovskiy, W. Tian, Y. K. Sung, W. Sun, J. L. Hsu, S. Manickam, D. Wagh, L. M. Joubert, G. L. Semenza, J. Rajadas and M. R. Nicolls, *Biomaterials*, 2014, **35**, 803–813.
60 L. Zhang, Y. Xiang, H. Zhang, L. Cheng, X. Mao, N. An, L. Zhang, J. Zhou, L. Deng, Y. Zhang, X. Sun, H. A. Santos and W. Cui, *Adv. Sci.*, 2020, **7**, 1903553.
61 D. Schmauss, A. Weinzierl, V. Schmauss and Y. Harder, *Eur. Surg. Res.*, 2018, **59**, 255–264.
62 R. G. Li, G. H. Ren, X. J. Tan, B. Yu and J. J. Hu, *Med. Sci. Monit.*, 2013, **19**, 510–517.
63 M. He, Q. Wang, Z. Shi, Y. Xie, W. Zhao and C. Zhao, *Colloids Surf., B*, 2017, **158**, 518–526.
64 R. Zhu, G. Wu, X. Liu, D. Shi, B. Cao, R. Gu, J. Xiao and H. Liao, *RSC Adv.*, 2015, **5**, 28023–28029.
65 L. P. Frazao, J. Vieira de Castro and N. M. Neves, *Adv. Exp. Med. Biol.*, 2020, **1250**, 109–124.
66 T. Khampieng, P. Aramwit and P. Supaphol, *Int. J. Biol. Macromol.*, 2015, **80**, 636–643.
67 D. W. Kim, H. S. Hwang, D. S. Kim, S. H. Sheen, D. H. Heo, G. Hwang, S. H. Kang, H. Kweon, Y. Y. Jo, S. W. Kang, K. G. Lee, K. W. Park, K. H. Han, J. Park, W. S. Eum, Y. J. Cho, H. C. Choi and S. Y. Choi, *BMB Rep.*, 2011, **44**, 787–792.
68 J. W. Kim, Y. Y. Jo, H. Y. Kweon, D. W. Kim and S. G. Kim, *Maxillofac. Plast. Reconstr. Surg.*, 2018, **40**, 10.
69 T. Mimae, T. Hirayasu, K. B. Kimura, A. Ito, Y. Miyata and M. Okada, *Gen. Thorac. Cardiovasc. Surg.*, 2010, **58**, 511–515.
70 H. Chen, P. Jia, H. Kang, H. Zhang, Y. Liu, P. Yang, Y. Yan, G. Zuo, L. Guo, M. Jiang, J. Qi, Y. Liu, W. Cui, H. A. Santos and L. Deng, *Adv. Healthcare Mater.*, 2016, **5**, 907–918.
71 Z. Hou, C. Nie, Z. Si and Y. Ma, *Diabetes Res. Clin. Pract.*, 2013, **101**, 62–71.
72 U. Hopfner, Z. N. Maan, M. S. Hu, M. M. Aitzetmuller, M. Zaussinger, M. Kirsch, H. G. Machens and D. Duscher, *J. Plast. Reconstr. Aesthet. Surg.*, 2020, **73**, 1738–1746.
73 S. Q. Gao, C. Chang, J. J. Li, Y. Li, X. Q. Niu, D. P. Zhang, L. J. Li and J. Q. Gao, *Drug Deliv.*, 2018, **25**, 1779–1789.

